Rapid Communications

Mass-transport properties of ternary Fe(C,O) alloys revealed by multicomponent cluster synergies

Thomas Schuler* and Maylise Nastar
DEN-Service de Recherches de Métallurgie Physique, CEA, Université Paris-Saclay, F-91191 Gif-sur-Yvette, France

Luca Messina
DEN-Service de Recherches de Métallurgie Physique, CEA, Université Paris-Saclay, F-91191 Gif-sur-Yvette, France and KTH Royal Institute of Technology, Nuclear Engineering, SE-114 21 Stockholm, Sweden

(Received 27 September 2019; accepted 30 January 2020; published 18 February 2020)

Understanding and quantifying mass-transport properties in multicomponent alloys poses the issues of (1) harvesting the atomic scale data, (2) setting up and solving a complex mathematical problem, and (3) identifying the underlying physics. This Rapid Communication demonstrates that the kinetic cluster expansion formalism associated with the open-source code KINECLUE provides the means to solve the last two issues. The efficiency of this framework is illustrated on the study of the temperature-composition dependence of the flux coupling properties in Fe(C), Fe(O), and Fe(C,O) alloys, with a particular emphasis on the synergetic effects between alloying elements.

DOI: 10.1103/PhysRevMaterials.4.020401

Mass transport controls the evolution towards equilibrium, microstructure metastability, local segregations, and phase transformations, and it is therefore at the core of materials understanding, development, usage, and aging. For instance, carburization and oxidation are concomitant phenomena in Fe alloys due to the gas mixtures used in industrial processes [1,2]. The knowledge of their relative kinetics is key to monitoring the final microstructure [3]. Yet, equilibrium is not always reached [4], and kinetics is also affected by the evolving microstructure and vacancy content [5]. Moreover, internal oxidation may produce vacancy fluxes [6,7], leading to flux coupling [8]. Mass transport in crystals occurs via atom and defect displacements so it is an atomic scale phenomenon, and true understanding lies at this scale, while the change of scale to a phenomenological description in terms of transport coefficients provides practical models for materials scientists.

The scale transfer procedure is a challenging, still open, mathematical problem which has been the focus of many studies since the beginning of the 20th century. Given a Markovian system represented by a set of configurations and transitions between these configurations, transport coefficients can be expressed as an average over all possible trajectories in the system, i.e., all combinations of successive transitions. The difficulty lies in the theoretically infinite number of these trajectories.

The integration over infinite trajectories is sometimes possible [9–12], but currently limited to simple systems. These solutions are elegant and mathematically exact, but diffusion is always limited in time and space in real-life materials, which indicates that infinite integration is not mandatory. Indeed, other methods use cutoff distances to limit the integration [13,14], and from a numerical point of view, the results are found very close to infinite integration for a sufficient cutoff distance because the weight of kinetic trajectories decreases with trajectory length. Hence, these simpler and more approximate models provide a fair compromise between computability, generality, and accuracy. Nevertheless, the number of trajectories to consider for a given cutoff distance is a fast increasing function of the number of alloy components.

To our knowledge, there is one example of an analytical calculation of solute diffusivity with a three-defect cluster in a binary alloy [15], while other studies were performed on infinitely dilute systems (containing monomers and pairs only) [16–29], and databases that are currently soaring reduce to these infinitely dilute systems [30–35].

Moreover, it was shown that small impurity concentrations may have large thermodynamic effects [36], and it is expected that the same happens for kinetic properties. Also, it is known that solute-defect clusters larger than pairs are the most probable cluster under certain conditions [37–39]. Ideal trapping (e.g., immobile clusters) is often assumed [40,41] but there are examples of clusters that are more mobile than monomer species [42,43]. Therefore, neglecting clusters larger than pairs is definitely questionable, but a model to evaluate their contribution to mass transport is missing.

This Rapid Communication presents an effective framework to quantify solute-point defect cluster contributions to the transport coefficients in binary and ternary alloys. The latter have not been treated at this level of precision while they are technologically relevant and show complex and rich kinetic phenomena. We focus on dilute systems but in terms of modeling capabilities our approach considers up to four interacting cluster components both in binary and ternary alloys. We describe the general approach, methods, and parametrization schemes, and then we apply those to

*Author to whom correspondence should be addressed: thomas.schuler@cea.fr

FeC, FeO, and FeCO dilute alloys and study the concentration effects on the flux coupling properties.

Our approach is based on a cluster expansion of the Onsager matrix [44]. It requires the alloying elements to be sufficiently dilute so that at each time the system can be well separated into subsystems (called clusters) and that this separation holds for a period of time long enough for clusters to reach local equilibrium between their various internal configurations. Under this assumption, cluster thermodynamic and kinetic properties are intrinsic equilibrium cluster properties and can be computed separately for each cluster. The separation is formally performed by setting a cutoff range called the kinetic radius [44] beyond which the trajectories of atoms and defects are assumed to be uncorrelated. This kinetic radius is typically a few lattice parameters in length (two in this study), and the corresponding concentration levels required to validate the above-mentioned assumption typically range between 0.1 and 1 at. %. Given the solubility limits of C and O in Fe [37], this assumption is completely reasonable for Fe(C,O) alloys.

The full kinetic properties of the system are obtained by summing all cluster contributions,

$$L_{\alpha\beta} = \sum_{l,m,n} [V_l X_m Y_n] L_{\alpha\beta}(V_l X_m Y_n), \tag{1}$$

where $L_{\alpha\beta}$ is a total transport coefficient which characterizes the whole system ($\alpha\beta$ component of the Onsager matrix [45]) and the sum runs over all cluster types $V_l X_m Y_n$ (l, m, n being the number of vacancies, solute X, and solute Y in the cluster, respectively). Each cluster type is characterized by concentration $[V_l X_m Y_n]$ (in m^{-3}) and cluster transport coefficients $L_{\alpha\beta}(V_l X_m Y_n)$ (in m^2/s). Here, these cluster transport coefficients are obtained using the KINECLUE code [44,46], which implements the self-consistent mean-field (SCMF) method [13,14,23] in an automated and efficient way, and cluster concentrations are computed with a low-temperature expansion (LTE) approach [36,47–51].

The LTE of the free energy is performed around a reference state (pure α-Fe), and each term in the expansion consists in adding vacancies (V) and/or solutes (X, Y). Rigorously speaking, the expansion is in terms of energy difference with respect to the reference system, but as solution and formation energies are large in these systems, the expansion is equivalently performed in terms of cluster sizes. The partition function of a $V_l X_m Y_n$ cluster reads $Z_{V_l X_m Y_n} = \sum_p g_p \exp(E_b^p / k_B T)$, where the sum runs over all internal configurations p of cluster $V_l X_m Y_n$, each one having its geometrical multiplicity g_p accounting for configurational entropy, and its binding energy E_b^p (positive value means attraction), k_B is the Boltzmann constant, and T the absolute temperature. Let us define $[\alpha] = \exp(\mu_\alpha / k_B T)$, μ_α being the chemical potential of species $\alpha = V, X, Y$. In the LTE formalism, the nominal solute concentration $[X]_T$ is expressed as

$$[X]_T = \sum_{l,m,n} m [V]^l [X]^m [Y]^n Z_{V_l X_m Y_n}, \tag{2}$$

and a similar expression holds for $[V]_T$ and $[Y]_T$.

The SCMF method uses statistical mechanics to compute transport coefficients from the knowledge of jump mechanisms and jump rates. Not only are first nearest-neighbor jumps considered in our calculations, but also second- and third-nearest-neighbor jumps of interstitial solutes around vacancies which happen to have small migration barriers in these alloys [43].

Our methodology requires atomic scale input, namely, binding energies for the LTE, and migration energies and attempt frequencies for the SCMF. Binding energies were taken from previously published *ab initio* data when available, or computed from a lattice interaction model fitted to ∼130 *ab initio* binding energies that was developed previously [37]. This model uses two-body and three-body interactions to capture the effect of local chemistry and local lattice relaxation. We used ∼45 previously computed *ab initio* migration energies [43], and the remaining barriers were estimated with a simple kinetically resolved activation barrier model [52] where the activation energies are taken as the migration energies of isolated solutes or vacancy, and attempt frequencies ν_α are taken constant for each species and obtained from fitted experimental data [23].

Irradiation maintains a supersaturation of point defects in the bulk, creating a sustained flux of point defects from the bulk to point defect sinks [53–55]. This point defect flux (only vacancies in this study) creates a coupled flux of solutes due to vacancy-solute interactions, and the magnitude of this coupled flux is characterized by the flux coupling ratio $\eta = L_{XV}/L_{VV}$, $X = \mathrm{C}, \mathrm{O}$. Obviously, if only solute and vacancy monomers are accounted for, $\eta = 0$. In a binary alloy, the infinitely dilute drag ratio η_∞ is obtained considering V, X, and VX clusters only,

$$\eta_\infty = \frac{L_{XV}(VX)/L_{VV}(VX)}{1 + \lambda_V/[X]}, \tag{3}$$

where $\lambda_{V_l X_m} = Z_{V_l X_m} L_{VV}(V_l X_m)/Z_{VX} L_{VV}(VX)$. Here, including concentration effects means including the mass-transport contribution of clusters larger than VX pairs, and we will show how these contributions change flux coupling properties by comparing η and η_∞.

The first-order concentration correction should include either VX_2 or V_2X clusters. In the Fe(C) alloy, $[V]_T \ll [\mathrm{C}]_T$ and the $V\mathrm{C}_2$ cluster is found particularly stable due to the formation of a covalent C-C bond in the vicinity of the vacancy [37,56–58]. Hence, as a first step, let us add the contribution from $V\mathrm{C}_2$ clusters only, and the drag ratio reads

$$\eta = \frac{[V\mathrm{C}] L_{\mathrm{CV}}(V\mathrm{C}) + [V\mathrm{C}_2] L\mathrm{C}(V\mathrm{C}_2)}{[V] L_{VV}(V) + [V\mathrm{C}] L_{VV}(V\mathrm{C}) + [V\mathrm{C}_2] L_{VV}(V\mathrm{C}_2)}. \tag{4}$$

Denoting $\chi_{V_l X_m} = Z_{V_l X_m} L_{XV}(V_l X_m)/Z_{VX} L_{VX}(VX)$ and $\tilde{\lambda}_l = [V]^{l-1}([X]\lambda_{V_l X} + \lambda_{V_l})$, Eq. (4) is recast into

$$\frac{\eta}{\eta_\infty} = \frac{1 + [\mathrm{C}]\chi_{V\mathrm{C}_2}}{1 + [\mathrm{C}]^2 \lambda_{V\mathrm{C}_2}/\tilde{\lambda}_1}. \tag{5}$$

Note that $\lambda_{V_l X_m}$ and $\chi_{V_l X_m}$ are ratios of intrinsic cluster properties. The top plot of Fig. 1 shows a drastic effect of $V\mathrm{C}_2$ clusters on the drag ratio as η and η_∞ have opposite signs for $T < 410$ K. In Fe(C) alloys supersaturated with vacancies at room temperature, the infinitely dilute model would suggest a decrease of C segregation at point defect sinks, whereas a more comprehensive model including $V\mathrm{C}_2$ clusters yields the opposite conclusion.

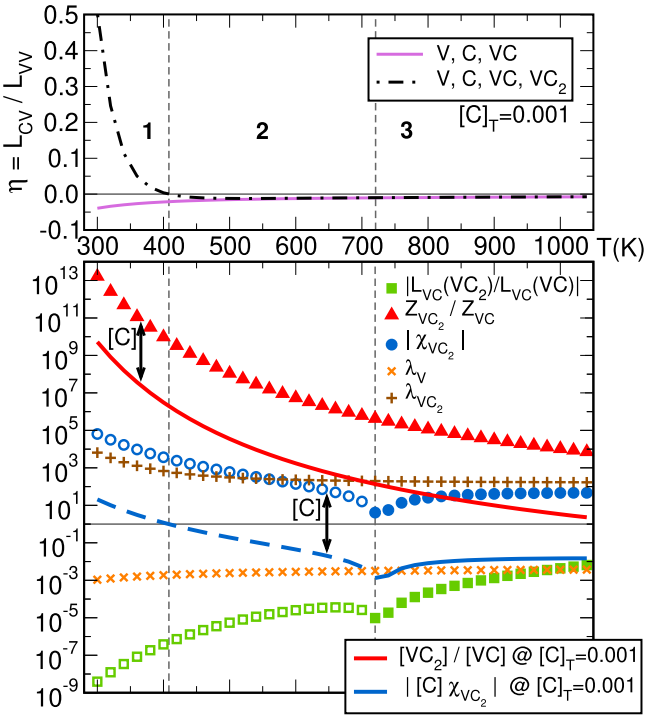

FIG. 1. Top: Drag ratio η as a function of temperature with/without the contribution from VC_2 clusters at $[C]_T = 10^{-3}$. Bottom: Various ratios of cluster quantities as a function of temperature. The ones in the bottom legend depend on $[C]_T$ while the ones in the top legend are combinations of intrinsic cluster properties. All curves are independent of $[V]_T$. Open symbols and dashed lines represent negative quantities.

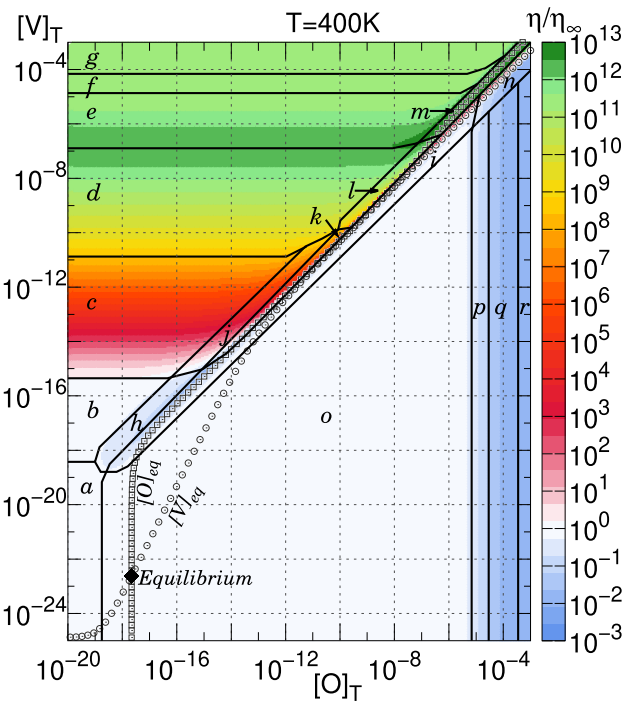

FIG. 2. Drag ratio in the FeO alloy compared with the infinitely dilute case as a function of vacancy and oxygen concentration at $T = 400$ K. The plot is split into several regions, each corresponding to different dominating cluster contributions to total concentrations and transport coefficients, as shown in Table I. The open squares show the O solubility limit as a function of $[V]_T$ and the open circles show the equilibrium vacancy concentration as a function of $[O]_T$. The black diamond symbol marks the equilibrium point [36,37].

Over the whole temperature range, there are more VC_2 clusters than VC clusters (red line), but the latter diffuse much faster than the former (green symbols) leading to a competition between thermodynamics and kinetics. In region 1, the (positive) VC_2 contribution prevails in L_{VC}. In regions 2 and 3, the (negative) VC contribution prevails in L_{VC} despite the fact that most C atoms are found in VC_2 clusters.

The $|\chi_{VC_2}|$ curve shows that there will be no concentration effects unless the solid solution is supersaturated with C, for instance, $[C]_T > 10^{-5}$ at $T = 300$ K or $T < 500$ K at $[C]_T = 10^{-3}$, which are largely above solubility limits at these temperatures [37,59,60].

Fe(O) alloys show two specific features: a very low O solubility limit (see Ref. [37] and references therein) and a very strong V-O binding energy (1.43 eV [37,61–63]). From a kinetic point of view, it was proposed that V_3O clusters could contribute significantly to the alloy kinetic properties since the O atom stabilizes the trivacancy while still allowing it to diffuse rapidly [43]. However, the kinetic properties of V_lO_m clusters were not fully accounted for, as the mobility of these clusters was estimated from one low-energy migration path only.

With KINECLUE [46] we are now able to go much further and compute the full transport coefficient matrices for a whole set of clusters, taking into account kinetic correlations. We considered clusters V, V_2, V_3, O, O_2, O_3, VO, VO_2, V_2O, and V_3O, and η/η_∞ reads

$$\frac{\eta}{\eta_\infty} = \frac{1 + [O]\chi_{VO_2} + [V](\chi_{V_2O} + [V]\chi_{V_3O})}{1 + ([O]^2\lambda_{VO_2} + \tilde{\lambda}_2 + \tilde{\lambda}_3)/\tilde{\lambda}_1}. \quad (6)$$

Figure 2 shows the evolution of this ratio as a function of $[O]_T$ and $[V]_T$ at $T = 400$ K.

There are three main regions in Fig. 2: the white region around the equilibrium point where flux coupling happens essentially as if the system was infinitely dilute (the contribution from VO pairs prevails); the blue region on the right-hand side where $\eta \ll \eta_\infty$; and the colored region from red to yellow to green where $\eta \gg \eta_\infty$. Contrary to Fe(C) alloys, all clusters considered here produce positive flux coupling, but the variation in terms of magnitude is much higher in Fe(O) alloys. These large variations stem from the interplay between cluster thermodynamics (V_lO_m clusters are very stable) and cluster kinetics (apart from V_3 and V_3O, V_lO_m clusters diffuse slowly). The plot is divided further into 18 regions labeled from "a" to "r," each having a specific combination of dominant clusters for nominal concentrations and transport coefficients, as detailed in Table I. The complexity of Fig. 2 demonstrates that cluster thermodynamic and kinetic properties must necessarily be considered concurrently to explain the variations of flux coupling properties over the full composition range.

To study the ternary Fe(C,O) alloy, we considered all V_lO_m clusters from the previous example and added clusters C, C_2, C_3, VC, V_2C, VC_2, V_3C, OC, O_2C, OC_2, and VOC. The

TABLE I. Dominating clusters in each region of Fig. 2. Columns $[V]_T$ and $[O]_T$ show the largest cluster contribution in the total concentration of vacancies and oxygen atoms, respectively. Columns L_{VV} and L_{OV} show the largest cluster contribution in the transport coefficients.

Region	$[V]_T$	$[O]_T$	L_{VV}	L_{OV}	Region	$[V]_T$	$[O]_T$	L_{VV}	L_{OV}
a	V	O	V	VO	j	V	VO_2	V	V_3O
b	V	VO	V	VO	k	VO_2	VO_2	V	V_3O
c	V	VO	V	V_3O	l	V_2O	VO_2	V	V_3O
d	V	V_2O	V	V_3O	m	V_2O	V_2O	V_3O	V_3O
e	V	V_2O	V_3	V_3O	n	VO_2	VO_2	VO_2	VO_2
f	V_3	V_2O	V_3	V_3O	o	VO_2	O	V	VO
g	V_3	V_3O	V_3	V_3O	p	VO_2	O	VO_2	VO
h	V	VO_2	V	VO	q	VO_2	O	VO_2	VO_2
i	VO_2	VO_2	V	VO	r	VO_2	O_3	VO_2	VO_2

latter cluster is particularly interesting because it contains all three species. The three off-diagonal coefficients of the VOC cluster Onsager matrix are all positive below 600 K, whereas above that temperature, $L_{VC}(VOC)$ and $L_{OC}(VOC)$ become negative, so the same cluster generates both positive and negative flux coupling.

Figure 3 shows two flux coupling coefficients at 500 K for both equilibrium vacancy concentration and constant supersaturated vacancy concentration. In the latter case there is a thermodynamic competition between C and O atoms to bind with the limited number of available vacancies, leading to abrupt changes in species chemical potentials. This thermodynamic effect modifies the full cluster distribution and explains the seeming discontinuities in kinetic properties.

At equilibrium vacancy concentration and O concentration larger than 3×10^{-9}, VO_2 clusters provide the main contribution to both L_{VV} and L_{OV} coefficients. Hence the total drag ratio can be approximated by the VO_2 cluster drag ratio which is close to 2 because in this strongly bound cluster, the V drags two O atoms. At lower O concentration, the isolated V contribution prevails in the L_{VV} coefficient and since this cluster does not contribute to flux coupling, the total drag ratio decreases. We observe a similar behavior for a supersaturation of vacancies, except that the threshold O concentration value is higher, and that at low O concentration, other vacancy-rich clusters are involved. Except at high $[C]_T$ and low $[O]_T$, both L_{VV} and L_{OV} coefficients are dominated by V_lO_m clusters so the effect of C on the L_{OV}/L_{VV} drag ratio is negligible.

For the L_{CV}/L_{VV} drag ratio, there is a change in sign as $[O]_T$ increases because VOC $[L_{CV}(VOC) > 0]$ dominates

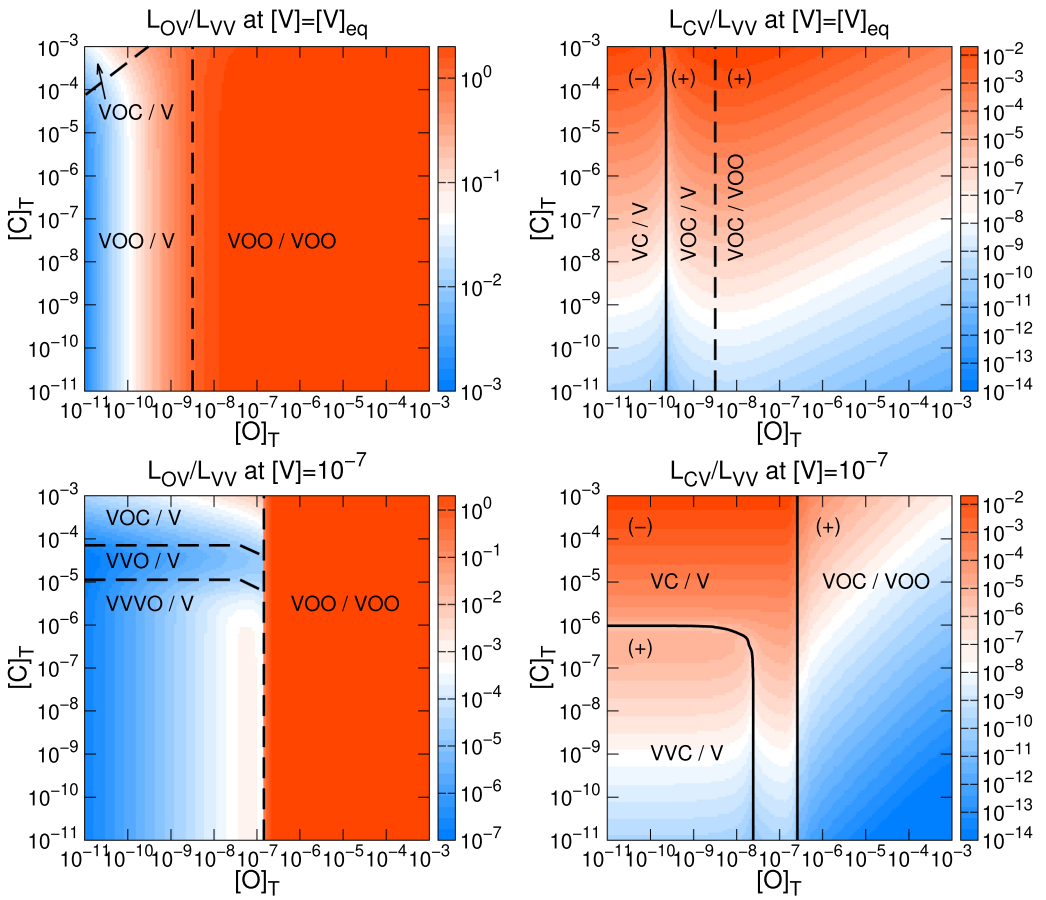

FIG. 3. Examples of flux coupling coefficients in the ternary Fe(C,O) alloy for equilibrium and supersaturated vacancy concentration at $T = 500$ K. Coefficients of the first column are always positive, while the sign is indicated for the second column, and we plot the absolute value. For each region we indicated the cluster having the main contribution to the off-diagonal coefficient, and the cluster having the main contribution to the L_{VV} coefficients, both separated by a "/" sign.

over VC [$L_{CV}(VC) < 0$]. For supersaturated vacancies and while isolated V dominate the L_{VV} coefficient, the magnitude of the L_{CV}/L_{VV} ratio is independent of $[O]_T$ because V_lC_n clusters prevail in both coefficients. Nevertheless, $[O]_T$ controls the sign of flux coupling by binding with vacancies and thereby reducing the concentration of V_2C clusters [$L_{CV}(V_2C) > 0$] in favor of VC clusters. For $[O]_T > 2 \times 10^{-7}$, the flux coupling ratio decreases with $[O]_T$ and increases with $[C]_T$, which is understandable once the dominating clusters are known.

We presented a framework aiming at computing and rationalizing the mass-transport properties of dilute multicomponent systems. Our methodology relies on intrinsic thermodynamic and kinetic properties of clusters, which are computed combining *ab initio* calculations and the KINECLUE code. The decomposition of the Onsager matrix into cluster contributions is a powerful and practical approach to the extreme complexity of diffusion in multicomponent alloys.

Taking into account clusters larger than pairs, our study sheds light on the flux coupling properties of dilute Fe alloys. Assuming that the system is locally at equilibrium, thermodynamics controls the cluster population, and abrupt changes occur at some threshold solute concentration values. Then, knowing the intrinsic kinetic properties of each cluster, the kinetic properties of a given cluster population can be computed and analyzed. We found that quite often, the most thermodynamically stable cluster is not the one controlling flux coupling, as shown, for instance, in Fe(C) and Fe(C,O) alloys.

Our methodology is a general and effective tool to go from atomic jump frequencies to continuous transport coefficients. The study of the sensibility of our model to atomic scale input (binding and migration energies) is beyond the aim of our study, but KINECLUE does provide the tools to perform such an analysis, as it was done in dilute FeC alloys, for instance [44]. The cluster formalism makes it possible to study dilute multicomponent systems that are closer to real-life materials and home to richer and more diverse physical phenomena. Moreover, the outputs of our framework are thermodynamic and kinetic properties of clusters, which turn out to be the inputs required for cluster dynamics simulations (e.g., Ref. [64]). The concentrations computed at steady state with low-temperature expansions in this study could be obtained as a function of time with cluster dynamics, enabling quantitative predictions of time-dependent thermodynamic and kinetic properties in transient systems.

[1] R. Chatterjee-Fischer, Metall. Trans. A **9**, 1553 (1978).
[2] J. Shen, S. Liu, X. Guo, and Y. Niu, Corros. Sci. **129**, 1 (2017).
[3] H. J. Grabke, Mater. Corros. **56**, 384 (2005).
[4] M. Romedenne, F. Rouillard, D. Hamon, B. Malard, and D. Monceau, Corros. Sci. **159**, 108147 (2019).
[5] A. Chakrabarty, E. T. Bentria, S. A. Omotayo, O. Bouhali, N. Mousseau, C. S. Becquart, and F. E. Mellouhi, Appl. Surf. Sci. **491**, 792 (2019).
[6] A. Uedono, M. Muramatsu, T. Ubukata, M. Watanabe, T. Ichihashi, R. Suzuki, T. Ohdaira, T. Mikado, and S. Takasu, J. Appl. Phys. **89**, 3606 (2001).
[7] S. Perusin, B. Viguier, D. Monceau, L. Ressier, and E. Andrieu, Acta Mater. **52**, 5375 (2004).
[8] T. R. Anthony, Acta Metall. **18**, 307 (1970).
[9] G. L. Montet, Phys. Rev. B **7**, 650 (1973).
[10] M. Koiwa and S. Ishioka, Philos. Mag. A **47**, 927 (1983).
[11] J. Bocquet, Philos. Mag. **94**, 3603 (2014).
[12] D. R. Trinkle, Philos. Mag. **97**, 2514 (2017).
[13] M. Nastar, V. Y. Dobretsov, and G. Martin, Philos. Mag. A **80**, 155 (2000).
[14] M. Nastar, Philos. Mag. **85**, 3767 (2005).
[15] J. Bocquet, Philos. Mag. **95**, 394 (2015).
[16] V. Barbe and M. Nastar, Philos. Mag. **87**, 1649 (2006).
[17] D. A. Andersson, B. P. Uberuaga, P. V. Nerikar, C. Unal, and C. R. Stanek, Phys. Rev. B **84**, 054105 (2011).
[18] S. Ganeshan, L. Hector, and Z.-K. Liu, Acta Mater. **59**, 3214 (2011).
[19] T. Garnier, V. R. Manga, D. R. Trinkle, M. Nastar, and P. Bellon, Phys. Rev. B **88**, 134108 (2013).
[20] T. Garnier, V. R. Manga, P. Bellon, and D. R. Trinkle, Phys. Rev. B **90**, 024306 (2014).
[21] A. Allnatt, I. Belova, and G. Murch, Philos. Mag. **94**, 2487 (2014).
[22] L. Scotti and A. Mottura, J. Chem. Phys. **142**, 204308 (2015).
[23] T. Schuler and M. Nastar, Phys. Rev. B **93**, 224101 (2016).
[24] A. Claisse, T. Schuler, D. A. Lopes, and P. Olsson, Phys. Rev. B **94**, 174302 (2016).
[25] E. Vathonne, D. A. Andersson, M. Freyss, R. Perriot, M. W. D. Cooper, C. R. Stanek, and M. Bertolus, Inorg. Chem. **56**, 125 (2016).
[26] H. H. Wu, P. Wisesa, and D. R. Trinkle, Phys. Rev. B **94**, 014307 (2016).
[27] R. Agarwal and D. R. Trinkle, Phys. Rev. Lett. **118**, 105901 (2017).
[28] J.-L. Bocquet, C. Barouh, and C.-C. Fu, Phys. Rev. B **95**, 214108 (2017).
[29] D. Andersson, X.-Y. Liu, B. Beeler, S. Middleburgh, A. Claisse, and C. Stanek, J. Nucl. Mater. **515**, 312 (2019).
[30] L. Messina, M. Nastar, N. Sandberg, and P. Olsson, Phys. Rev. B **93**, 184302 (2016).
[31] B.-C. Zhou, S.-L. Shang, Y. Wang, and Z.-K. Liu, Acta Mater. **103**, 573 (2016).
[32] H. Wu, A. Lorenson, B. Anderson, L. Witteman, H. Wu, B. Meredig, and D. Morgan, Comput. Mater. Sci. **134**, 160 (2017).
[33] S. S. Naghavi, V. I. Hegde, and C. Wolverton, Acta Mater. **132**, 467 (2017).
[34] H.-J. Lu, H. Wu, N. Zou, X.-G. Lu, Y.-L. He, and D. Morgan, Acta Mater. **154**, 161 (2018).
[35] R. Agarwal and D. R. Trinkle, Acta Mater. **150**, 339 (2018).
[36] T. Schuler, C. Barouh, M. Nastar, and C.-C. Fu, Phys. Rev. Lett. **115**, 015501 (2015).

[37] C. Barouh, T. Schuler, C.-C. Fu, and M. Nastar, Phys. Rev. B **90**, 054112 (2014).
[38] D. Tanguy, Y. Wang, and D. Connétable, Acta Mater. **78**, 135 (2014).
[39] D. Connétable and M. David, J. Alloys Compd. **748**, 12 (2018).
[40] R. Oriani, Acta Metall. **18**, 147 (1970).
[41] J. Svoboda and F. Fischer, Acta Mater. **60**, 1211 (2012).
[42] C.-C. Fu, J. D. Torre, F. Willaime, J.-L. Bocquet, and A. Barbu, Nat. Mater. **4**, 68 (2004).
[43] C. Barouh, T. Schuler, C.-C. Fu, and T. Jourdan, Phys. Rev. B **92**, 104102 (2015).
[44] T. Schuler, L. Messina, and M. Nastar, Comput. Mater. Sci. **172**, 109191 (2019).
[45] L. Onsager, Phys. Rev. **37**, 405 (1931).
[46] T. Schuler, L. Messina, and M. Nastar, KINECLUE v1.0 GitHub repository, 2019, https://github.com/lukamessina/kineclue.
[47] C. Domb, in *Phase Transitions and Critical Phenomena*, edited by C. Domb and M. S. Green, Vol. 3 (Academic, New York, 1974), p. 425.
[48] F. Ducastelle, *Order and Phase Stability in Alloys*, Cohesion and Structure Vol. 3 (North-Holland, Amsterdam, 1991).
[49] Y. L. Bouar, A. Loiseau, and A. Finel, Phys. Rev. B **68**, 224203 (2003).
[50] E. Clouet and M. Nastar, Phys. Rev. B **75**, 132102 (2007).
[51] T. Schuler, F. Christien, P. Ganster, and K. Wolski, Appl. Surf. Sci. **492**, 919 (2019).
[52] A. V. der Ven and G. Ceder, Phys. Rev. Lett. **94**, 045901 (2005).
[53] T. Anthony, *Diffusion in Solids* (Elsevier, Ansterdam, 1975), pp. 353–379.
[54] M. Nastar and F. Soisson, *Comprehensive Nuclear Materials* (Elsevier, Amsterdam, 2012), pp. 471–496.
[55] A. J. Ardell and P. Bellon, Curr. Opin. Solid State Mater. Sci. **20**, 115 (2016).
[56] C. Domain, C. S. Becquart, and J. Foct, Phys. Rev. B **69**, 144112 (2004).
[57] C. C. Fu, E. Meslin, A. Barbu, F. Willaime, and V. Oison, Solid State Phenom. **139**, 157 (2008).
[58] A. T. Paxton and C. Elsässer, Phys. Rev. B **87**, 224110 (2013).
[59] J. Chipman, Metall. Mater. Trans. B **3**, 55 (1972).
[60] J. Merlin, P. Merle, S. Garnier, M. Bouzekri, and M. Soler, Metall. Mater. Trans. A **35**, 1655 (2004).
[61] C. L. Fu, M. Krčmar, G. S. Painter, and X.-Q. Chen, Phys. Rev. Lett. **99**, 225502 (2007).
[62] Y. Jiang, J. R. Smith, and G. R. Odette, Phys. Rev. B **79**, 064103 (2009).
[63] A. Claisse and P. Olsson, Nucl. Instrum. Methods Phys. Res., Sect. B **303**, 18 (2013).
[64] T. Jourdan, G. Bencteux, and G. Adjanor, J. Nucl. Mater. **444**, 298 (2014).